INSTITUTE OF PHYSICS PUBLISHING JOURNAL OF PHYSICS B: ATOMIC, MOLECULAR AND OPTICAL PHYSICS

J. Phys. B: At. Mol. Opt. Phys. **38** (2005) 3535–3545

New measurements of absolute total cross sections for electron impact on caesium using a magneto-optical trap

M Łukomski[1,2], J A MacAskill[3], D P Seccombe[1], C McGrath[4], S Sutton[1], J Teeuwen[1], W Kedzierski[1], T J Reddish[1], J W McConkey[1] and W A van Wijngaarden[5]

[1] Department of Physics, University of Windsor, Ontario N9B 3P4, Canada
[2] Instytut Fizyki, Uniwersytet Jagielloński, ul. Reymonta 4, 30-059 Kraków, Poland
[3] Jet Propulsion Laboratory, California Institute of Technology, 6800 Oak Grove Dr, Pasadena, CA 91109, USA
[4] Northern Ireland Regional Medical Physics Agency, Royal Victoria Hospital, Belfast BT12 6BA, UK
[5] Department of Physics, York University, Ontario, Canada

Received 16 June 2005, in final form 22 August 2005
Published 14 September 2005

Abstract

A new magneto-optical trap designed specifically for the measurement of absolute electron impact cross sections is described. Experimental results for electron impact total cross sections involving 6^2S ground state Cs are presented over the energy range 5–200 eV. Significant disagreement is obtained between our experimental data and convergent close coupling (CCC) or Breit–Pauli R-matrix calculations at the lower energies. Above 100 eV our data overlap earlier measurements from this laboratory made with a completely different apparatus and agree well with the CCC results. A comparison is made with other measurements using more conventional techniques.

1. Introduction

The measurement of electron impact cross sections involving atomic and molecular targets continues to provide important data for a large variety of applications. Increasingly sophisticated techniques, both experimental and theoretical, are being applied to meet the demands of basic research and high-technology industry. In this work the trap-loss technique, first developed by Lin and co-workers [1–3], is used to determine total cross sections from the fluorescence decays of the trapped atoms, with and without an electron beam present. The loss of atoms from the trap, due to electron collisions, is related directly to the cross section and electron flux through the trap. Knowledge of the absolute target density is not required. Furthermore, because the act of trapping results in the preparation of a target with a large fraction of excited species, it is possible to obtain absolute cross section data for

excited species. Consequently, the use of a magneto-optical trap (MOT) for collision cross section measurements can offer a number of advantages over more conventional techniques. Moreover, there is great interest in such absolute cross section data, particularly from the plasma physics and industrial communities [4].

To date most MOT measurements have involved alkali targets because of the availability of suitable trapping lasers. We have concentrated our efforts on caesium. This is perhaps the most interesting alkali target because of potential practical applications, such as in atomic clocks or ion propulsion schemes for space vehicles. Further, being the heaviest of the alkalis, caesium is also of great interest from a theoretical point of view because relativistic and atomic structure effects should be significant [5].

Total cross section measurements in Cs, prior to 1996, were summarized by Zecca *et al* [6]. They are those of Visconti *et al* [7], which cover the energy range 0.3–9 eV, those of Jaduszliwer and Chan [8], which cover the range 2–18 eV and the very early data of Brode [9] in 1929, which extended up to 400 eV. As pointed out by Zecca *et al* [6] and by Bederson and Kieffer [10] in an early review, serious questions existed about the Brode data which seemed to be too high by a factor of at least 2. Since 1996 there have been two further sets of measurements. MacAskill *et al* [5] used a MOT and presented data which confirmed that the early Brode data [9] were in serious error below 100 eV. Their theoretical results covered the energy range 0.3–400 eV for scattering both from the 6^2S ground state and the 6^2P excited state. Excellent agreement between convergent close coupling (CCC) theory and experiment was demonstrated in the region of overlap above 100 eV. Finally, there have been some measurements by Surdutovich *et al* [11] covering the range 6–200 eV. These lie slightly lower (10%) than the Jaduszliwer and Chan results below 15 eV, where comparison is possible. Their higher energy data (above 100 eV) confirm the work of MacAskill *et al* [5].

For completeness we mention the other electron impact collision studies involving MOTs. Huang *et al* [12, 13] have made a detailed study of ionization using lithium targets and Uhlmann *et al* [14] have measured total cross sections from metastable helium. A comprehensive review of the various techniques needed for measuring different types of cross sections using MOTs is available [15].

Our earlier studies [5] covered a 100–400 eV energy range for the incident electrons. We have since developed a completely new apparatus with many significant changes from our earlier work. These have resulted in a more efficient data acquisition rate and have enabled us to extend the energy range down to 5 eV. This low energy capability is important, as it is in this region that discrepancies between the earlier experimental work and theory become apparent.

2. Experimental method

2.1. Principle of method

When a collection of trapped atoms is irradiated by a beam of electrons and collisions occur, momentum is transferred to the atoms which may cause them to be ejected from the trap. Atoms are ejected from the trap due to the electron–atom collisions at a rate

$$\Gamma_e = \sigma J/e \tag{1}$$

where σ is the cross section for ejecting atoms from the trap, J is the electron current density and e is the electronic charge. The measurements of Γ_e and J yield σ directly. For very small scattering angles where the transfer of momentum in the collision is below some limiting value, the collision will not be violent enough to remove the atom from the trap. This issue has been discussed by Schappe *et al* [1, 15], Uhlmann *et al* [14] and MacAskill *et al* [5]

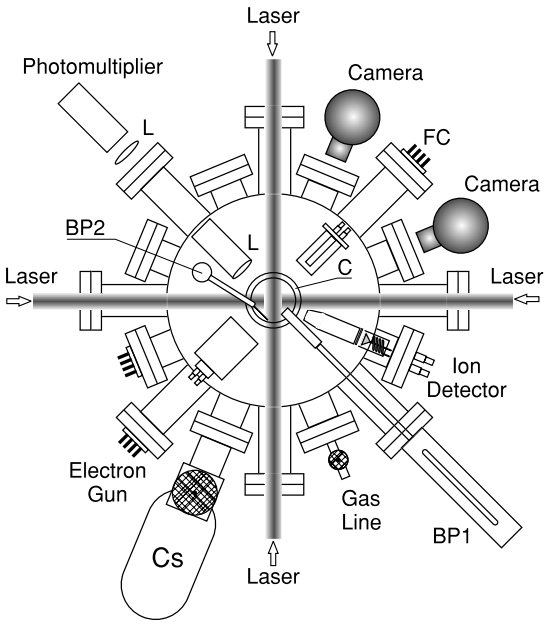

Figure 1. Schematic diagram of the vacuum chamber showing the lay-out of components in the *x*–*y* plane. FC, Faraday cup system; BP1, BP2, beam probes; Cs, caesium reservoir; L, lens, C, anti-Helmholtz coils. Two further counter propagating laser beams perpendicular to the plane of picture (intersecting the other laser beams in the centre of the chamber) are not shown on the diagram.

for absolute cross section measurements in trapped rubidium, metastable helium and caesium atoms, respectively. Calculations show that for our system (laser beam diameter, timing sequence, etc) with elastically scattered electrons of 5 eV energy, electrons scattered at angles smaller than about 5° will not impart enough momentum to eject atoms from the trap. As the impact energy increases, the differential cross sections become increasingly peaked around 0°; however, the ranges of low angle scattering, which result in no contribution to the loss of atoms from the trap, become much smaller and at 100 eV is ∼1°. The partial cancellation of these two effects has been discussed by Schappe *et al* [15]; their contribution to the present experiment will be considerably less than the measurement uncertainty.

2.2. Experimental technique

Many of the experimental details relevant to measuring cross sections in MOTs have been given elsewhere [5, 15] and so will not be repeated here. Only the major modifications to our original system, which are relevant to the present work, will be discussed. A block diagram of the apparatus is shown in figure 1.

The MOT is of a standard design [1, 16–18]. It consists of a stainless-steel, ultrahigh vacuum chamber evacuated with ion and turbo pumps that provide a typical operating pressure in the low 10^{-8} Torr region. The anti-Helmholtz pair of coils providing the magnetic trapping field is discussed below. They provide an axial field gradient of approximately 10 G cm^{-1} for an operating current of 2 A. A specially designed pulsing circuit is used with the magnetic trapping coils to allow the current to be switched rapidly by a TTL signal. This circuit also

provides a means of rapidly dissipating the coil current to minimize the decay time (<1 ms) of the magnetic field during switching.

Laser cooling of the atoms is achieved with the use of two external-cavity, grating-stabilized, diode lasers (SDL Inc.). One laser is used for trapping and the other for the re-pumping of atoms that have ended up in a dark ground state. Further details with a schematic of the optical layout are given in our earlier publication [5]. Briefly, both lasers are designed for operation at 852 nm, and are capable of producing a peak output power of 100 mW. A portion of each beam is split off and directed to a saturated absorption spectroscopy set-up which is used for frequency stabilization. Each laser may be frequency stabilized by using a lock-in amplifier to fix the frequency to a feature of the Doppler-free spectrum obtained from the saturated absorption spectroscopy. In practice it was found that such frequency stabilization was unnecessary in the case of the re-pumping laser. After passing through some primary optics, each laser beam is collimated and magnified to a ∼17 mm diameter before being merged. This merged beam is then divided into three new beams of approximately equal intensity that are finally circularly polarized before entering—and being retro-reflected through—the chamber.

The vacuum chamber housing the new trap is a 10 in. internal-diameter vessel. This allows us to make the anti-Helmholtz coils smaller and mount them internally, thus achieving the same magnetic field strengths at much lower power levels. Using internal rather than external coils resulted in B-field switching times that were also significantly reduced, as eddy currents in the chamber walls were eliminated. The extra ports enabled us to make observation of the Cs atom cloud using two infrared sensitive cameras positioned in the same, horizontal, plane. This allowed accurate monitoring of the position of the atom cloud which was vital in ensuring proper overlap of the electron beam with the trapped atoms.

The multi-element electron gun was designed to produce a broad near-parallel beam in the 5–400 eV electron energy range. An oxide coated cathode was used and two pairs of electrostatic deflectors allowed accurate control and steering of the electron beam. A typical beam current was 70 μA. Since accurate knowledge of the current density in the region of the MOT was necessary, two movable, 0.010 diameter, wire probes were arranged so that the electron beam profile could be monitored in two dimensions in a plane perpendicular to the e-beam direction. After scanning the e-beam diameter the wire probes could be retracted so that they did not interfere with the trapping laser beams. At each electron energy the gun controls were optimized so that the two measured diameters were as similar as possible. The measured profiles were then compared with a theoretical model where uniform density over the cross-sectional area of the beam was assumed. An example of such a data set is shown in figure 2. As is evident from figure 2, quite good agreement between the measured and theoretical profiles is obtained. The diameter of the electron beam was kept approximately constant (at ∼10 mm) over the range of energies investigated.

The probe, which scanned the e-beam diameter vertically, could also be moved about 20 mm along the e-beam (using a two-dimensional manipulator), so that the vertical beam profile could be monitored at different positions along the beam. This was invaluable because it allowed a determination of how the beam profile changed with the distance from the gun exit, i.e. diverging or converging. This allowed the gun's performance to be optimized to create a near-parallel beam. The wire probes were also used in conjunction with the cameras to accurately fix the position of the electron beam with respect to the atom cloud. The electron beam could then be moved as necessary to ensure good overlap, which is essential for accurate cross section measurement. An interesting result of monitoring the e-beam diameter in two dimensions was the fact that the beam was not always cylindrically symmetric. This was especially the case at the lower electron energies.

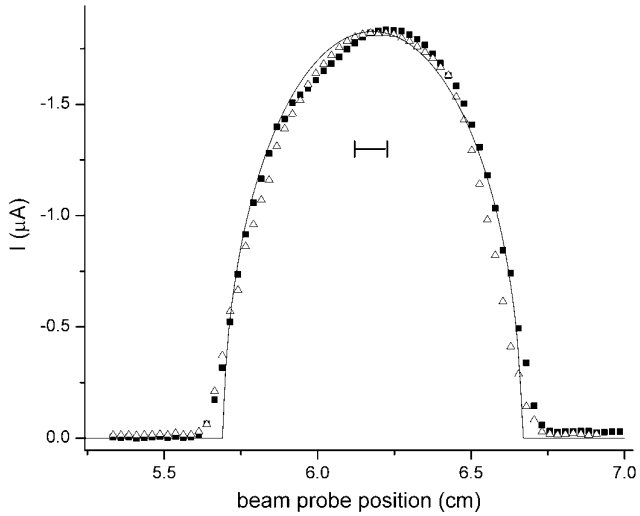

Figure 2. Typical electron beam profiles taken at an electron energy of 12.5 eV. Data points for the horizontal and vertical probes are indicated by filled squares and open triangles, respectively. The solid line is a theoretically derived profile assuming the cylindrical symmetry and uniform current density within the beam. The horizontal bar indicates the location and size of the trapped atom cloud within the beam profile.

A system of external coils is used to compensate for the earth's magnetic field and any other stray fields. This is very important especially for lower electron energies. They also provided some additional steering of the e-beam.

The Faraday cup system consists of inner and outer concentric cylindrical cups. The ratio of the currents measured on the inner and outer cups gives an indication of the size and alignment of the e-beam. Normally a small positive biasing voltage is used on the inner cup to avoid loss of secondary electrons. In order to ensure an accurate measurement of the total beam current, particularly at the lower electron energies where the e-beam diverged rapidly after traversing the interaction region, the following procedure was adopted. After each set of measurements of the trap loss rate (carried out as described below), the positive biasing of the Faraday cup system was increased until the measured current was observed to reach saturation. This ensured that the total current, which passed through the interaction region, was recorded. This information was used to calibrate the data obtained during routine measurements. At the higher electron energies this procedure also eliminated any problems due to secondary electron emission from collector surfaces. From the measurements of e-beam profile (discussed earlier) and total beam current, the current density, J, in the region of the atom cloud was obtained.

The MOT trapped atom fluorescence is collected and monitored continuously using a cooled EMI 9558 photomultiplier (PM) tube. As a significant improvement over our previous arrangement, a short focal length lens was installed inside the vacuum chamber with the atom cloud at its focus. This arrangement increased the aperture of the detection system while reducing the scattered background light. Thus we are able to increase significantly the signal-to-noise ratio in measurements and to make all measurements much faster (a crucial factor, particularly when working in the low electron energy range). The fluorescence from the trapped atoms was too large for direct photon counting to be feasible, without the use of suitable filters, and so the analogue output of the PM was digitized and monitored using

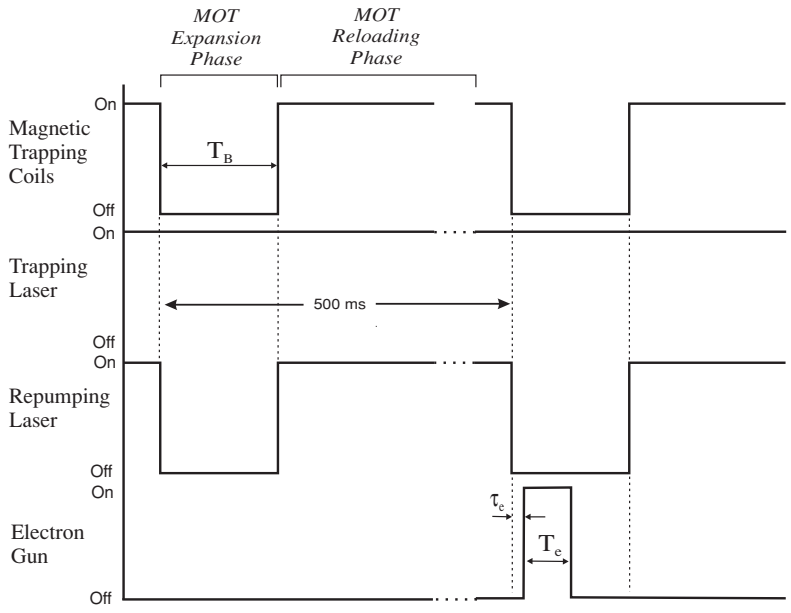

Figure 3. Experimental timing sequence. $\tau_e = 1$ ms; $T_e = 8$ ms; $T_B = 20$ ms.

a multichannel scaling plug-in card in the control computer. Thus the time variation of the trap fluorescence was recorded and displayed. Although large, light intensities were still well within the region where the PM output was linear with input intensity.

Since it is not possible to introduce the electron beam while the trapping magnetic field is on, the experiment proceeds in a pulsed mode. The timing sequence for this is shown in figure 3 and proceeds as follows. The trap is turned off for a time, T_B (20 ms), by switching off the magnetic field and the re-pumping laser. During alternate trap-off times an electron beam pulse is introduced for a time, T_e (8 ms), after a delay τ_e (1 ms) to ensure that the electrons are not perturbed as the magnetic field turns off. The value of (T_B–T_e) is chosen to be as large as reasonably possible to allow those atoms which have interacted with the electrons to escape the trap, without being so long as to empty the trap completely. The trap fluorescence is monitored continuously with the signals from alternate cycles being stored in separate memories. The time evolution of the trap fluorescence, both with and without the presence of the electron beam pulse, is obtained and processed as discussed later. The Faraday cup current is also continuously monitored.

All of the measurements presented here are determined by recording two fluorescence signals. The first is measured in the absence of the electron beam pulse, and is necessary to establish a 'reference' loss rate. This reference loss rate is a combination of factors including thermal expansion, inelastic collisions within the trap, gravitational acceleration, time-varying magnetic fields that occur during switching and collisions with vacuum residuals. The second signal is measured in the presence of the electron beam pulse, and displays a larger loss rate that includes the reference losses, mentioned earlier, and also losses due to electron collisions. These fluorescence signals are measured sequentially, as shown in the timing diagram, figure 3. This ensures consistency in trapping parameters during data collection and minimizes longer term variations in the reference fluorescence, electron beam current, laser intensity

and frequency detuning. Since, in this work, we are interested in cross sections involving ground state Cs atoms, the re-pumping laser is switched off prior to the introduction of the electron beam. The rapid optical pumping to a dark hyperfine level of the ground state occurs immediately, thus ensuring a total ground state target [5].

A final addition to this new apparatus was a detection system designed to perform measurements of Cs ions. This time-of-flight system consists of a 5 cm flight tube, followed by an acceleration mesh and a channeltron detector. This system is capable of measuring total Cs ion fluxes, created during the electron beam-trapped atom interaction, as well as distinguishing between Cs^+, Cs^{2+} and Cs^{3+}. Data obtained using this system will be presented in a future publication. In the present case this ionization detector was used to provide an accurate energy calibration for the e-beam. Helium was introduced into the vacuum system and the yield of He^+ ions was measured over the 23–33 eV incident electron energy range. The He^+ threshold at 24.58 eV was determined using a linear extrapolation and the error in the energy calibration was estimated to be ± 0.3 eV.

3. Data and error analysis

During continuous operation of the trap, in the absence of an electron beam, the trap population is given by

$$\frac{\mathrm{d}N}{\mathrm{d}t} = L - \Gamma N \tag{2}$$

for a loading rate L from the atomic vapour and a loss rate Γ out of the trap for all causes other than electron–atom collisions (mainly collisions with vacuum residuals). If equation (2) equals zero, then N describes the steady state population.

In the present method, the electrons interact with the caesium atoms only when the trapping forces are not present. Eliminating the trapping magnetic field and the output from the re-pumping laser, effectively removes any loading and so the term is dropped from the differential equation leaving

$$\frac{\mathrm{d}N}{\mathrm{d}t} = -\Gamma_0 N \tag{3}$$

where Γ_0 is the analogous loss rate to that in equation (2)—except the trapping forces are not present. In the presence of an electron beam, the loss rate in equation (3) is altered to $\Gamma_0 + \Gamma_e$, where Γ_e is the loss rate due to electronic collisions, presented in equation (1). From this, we obtain the following equations describing trap populations:

$$N(t) = N_0\,\mathrm{e}^{-\Gamma_0 t} \tag{4a}$$

$$\tilde{N}(t) = \tilde{N}_0\,\mathrm{e}^{-(\Gamma_0+\Gamma_e)t} \tag{4b}$$

where $N(t)$ and $\tilde{N}(t)$ describe the exponential decay of the trap populations as a function of time in the absence and presence of the electron beam, respectively.

To isolate the electron induced trap loss rate one takes the ratio of these two equations obtaining

$$\frac{N(t)}{\tilde{N}(t)} = \frac{N_0}{\tilde{N}_0}\,\mathrm{e}^{\Gamma_e t}. \tag{5}$$

Due to the long (500 ms) time period of our pulsing scheme (see figure 3), the steady state populations with and without the electron beam are the same, as shown at early times in figure 4 (between 0 and 10 ms); consequently, $N_0/\tilde{N}_0 \cong 1$. As the electron beam is present

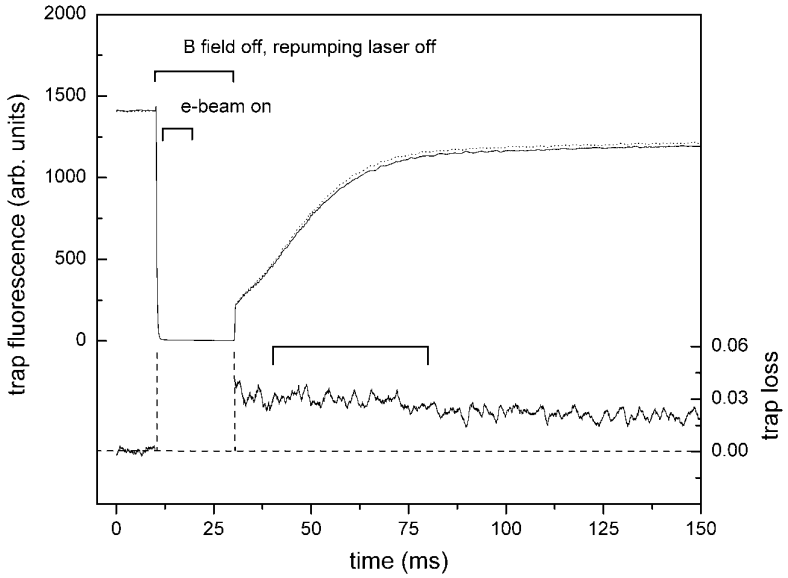

Figure 4. Typical fluorescence curves obtained after background subtraction. The solid (dashed) lines refer to data obtained with (without) the electron pulse. The lower curve is derived from the upper two and shows the logarithm of the measured trap population ratio with and without the electron interaction, which evolves in time during the reloading phase. The value immediately after switching on the magnetic field and re-pumping laser is equal to the trap loss, Γ_e (see text for details). The horizontal bar indicates the time interval, which is used to determine the average trap loss rate in this work.

for a time T_e (8 ms in this work), the loss rate is obtained directly from

$$\ln\left(\frac{N(T_e)}{\tilde{N}(T_e)}\right) = \Gamma_e T_e. \tag{6}$$

The measurement of the cross section for the ground state ($6^2S_{1/2}$) Cs requires the re-pumping laser to be off while the electron beam is pulsed on, to ensure that only the $6^2S_{1/2}$ state is populated [5]. As shown in figure 4, the re-pumping laser is switched off for T_B, along with the magnetic field. Following the removal of the re-pumping laser; we observe that the trap ceases to fluoresce in approximately 0.5 ms (see figure 4). Consequently, the trap is 'dark' during its expansion phase (i.e. while the magnetic field is off) during which time the electron beam is present for T_e. The value of Γ_e is measured using the fluorescence yield during the *reloading* phase.

While the actual response of the trap is not directly observable during the electron interaction time, the effect is reflected in the net difference of the trap populations during the initial reloading, as shown in figure 4. The difference in the fluorescence, observed at the beginning of the reloading phases for the electron beam off and on, is due solely to the electron collisions that occurred during the expansion phase. We note that for each measurement, evaluation of any background fluorescence (from untrapped atoms or scattered laser light) had to be carried out. This was obtained by repeating the measurements using the same timing sequence as in figure 3 but with the trapping magnetic field permanently off. By subtracting the resultant background signal we obtain the fluorescence yield due only to the population of trapped atoms. Figure 4 also shows the logarithm of the measured ratio of the trap populations,

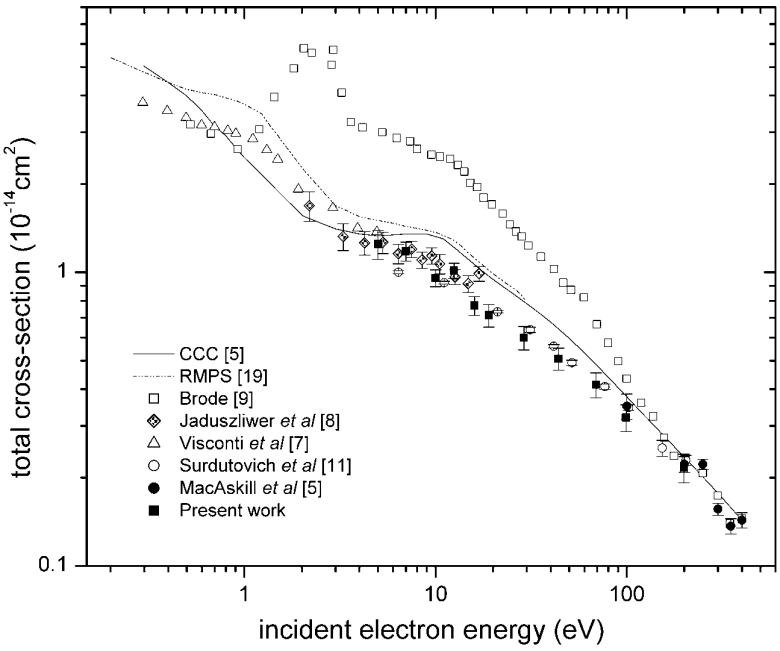

Figure 5. Measured and calculated Cs total cross sections as a function of electron energy.

with and without the electron beam present, as a function of time. Immediately after switching on the trapping magnetic field, the trap population ratio corresponds to that of equation (6). For improved accuracy we integrated the loss value over the 40 ms time interval shown in the figure to evaluate Γ_e. It should be noted that bringing the start of the integration window closer to the time that the trapping forces are turned on was observed to cause the signal to be prone to transient effects; extending the window in time eventually causes an underestimation in the measured loss rate. After 500 ms the trap has been reloaded and the cycle starts again. Normally we acquire data for 400 cycles to obtain the necessary statistical significance. At least 20 such measurements are averaged at each electron impact energy.

In the present experiment two quantities, the incident electron current density, J, and trap loss rate, Γ_e, caused by electron impact were determined and used to calculate the absolute cross section (see equation (1)). Both of these determinations required a number of separate measurements as discussed earlier. The error involved in each measurement was evaluated separately. The errors in Γ_e were largely statistical in nature with small systematic effects due to the positioning and stability of the atom cloud. The largest uncertainty in J arose from the determination of the size and detailed shape of the e-beam. The resultant uncertainties in J and Γ_e contribute, typically, $\sim$3% and $\sim$7%, respectively, to the uncertainty in the determination of σ (i.e. the trap loss uncertainty dominates). The uncertainties tabulated in the next section represent one standard deviation from the mean in each case.

4. Results and discussion

Figure 5 gives our experimental data for the total cross section out of the Cs $6^2S_{1/2}$ ground state. Also included are the data sets from [5, 7–9, 11, 19]. For convenience, our numerical data are

Table 1. Measured absolute total cross sections for electron collisions with ground state caesium. Estimated errors are given in the third column.

Energy (eV)	$\sigma(\times 10^{-15}\ \mathrm{cm}^2)$	$\Delta\sigma(\times 10^{-16}\ \mathrm{cm}^2)$
5	12.5	14
7	11.8	8.7
10	9.6	6.3
12.5	10.1	6.1
16	7.7	5.7
19	7.1	6.4
29	6.0	5.5
44	5.1	4.4
69	4.1	4.0
99	3.2	3.4
199	2.2	2.4

listed in table 1. A number of points are immediately evident. Very good agreement exists between all the high-energy experimental results (even those of Brode [9]) above 100 eV. Below 100 eV Brode's data are clearly spurious. Our data agree very well with those of Surdutovich *et al* [11] over the entire energy range covered by both data sets. Agreement with the early data of Jaduszliwer and Chan [8] in the region below 20 eV is also very good. The Jaduszliwer and Chan [8] datum point at 18 eV, which suggested a possible upward trend to the cross section as the energy was increased above this value, appears to be anomalous.

With the convergence of the experimental results obtained using three very different techniques, it is possible to assess the accuracy of the calculations. Figure 5 suggests that although the CCC calculations [5] yield accurate data at the higher energies, this is not the case as the energy is reduced below 75 eV. Divergence from experiment continues down to at least 5 eV. The *R*-matrix with pseudo-states (RMPS) calculations of Bartschat [19] and, particularly the CCC results [5] indicate a 'shoulder' in the cross section at around 10 eV. This feature is largely absent from the experimental data. Below 9 eV the two theoretical curves diverge from one another. Some of this divergence is possibly due to structure differences or inner shell effects. It is an unavoidable fact that with increasing complexity of the target, the structure approximations become of increasing importance relative to the scattering approximations.

Bartschat [20] obtained calculated values for the main contributions to the total cross section as a function of energy. From these data the following facts are evident. Below approximately 7 eV, elastic scattering provides the largest contribution to the total cross section. Above that energy, excitation of the 6p levels quickly dominates with smaller contributions from excitation of 5d and other discrete levels and from ionization. The presence of the 'shoulder' in the theoretical data in the region of 10 eV is due largely to a broad maximum in the 6p cross section near that energy with an additional, smaller, contribution from elastic scattering. Bartschat's calculations of the 6p cross section are in quite good agreement with the measurements of Chen and Gallagher [21] in the 10–30 eV region. Thus the observed differences between theory and experiment for the total cross section near 10 eV are most likely due to an overestimation of the calculated elastic scattering contribution.

5. Conclusions

Data have been presented on total electron scattering cross sections from Cs in its ground, 6^2S, state over an energy range from 5 to 200 eV. Excellent agreement is obtained with

earlier measurements taken using entirely different experimental set-ups. All the experimental measurements except the very early data of Brode [9] are essentially in harmony with one another. Good agreement between calculations and experiment is obtained at energies larger than about 75 eV but, below that energy down to about 5 eV, theory consistently overestimates the cross section.

Acknowledgments

We are pleased to acknowledge financial support from CIPI (the Canadian Institute for Photonic Innovation), CFI (the Canadian Foundation for Innovation), ONF (the Ontario Innovation Fund) and NSERC (Natural Sciences and Engineering Research Council of Canada). Helpful input from the mechanical and electronic shops at Windsor is gratefully acknowledged, as are very helpful discussions with Klaus Bartschat.

References

[1] Schappe R S, Feng P, Anderson L W, Lin C C and Walker T 1995 *Europhys. Lett.* **29** 439
[2] Schappe R S, Walker T, Anderson L W and Lin C C 1996 *Phys. Rev. Lett.* **76** 4328
[3] Keeler M L, Anderson L W and Lin C C 2000 *Phys. Rev. Lett.* **85** 3353
[4] Becker K H *et al* 2000 Electron-driven processes: scientific challenges and technological opportunities *US DOE Report*, Stevens Institute of Technology
[5] MacAskill J A, Kedzierski W, McConkey J W, Domyslawska J and Bray I 2002 *J. Electron Spectrosc. Relat. Phenom.* **123** 173
[6] Zecca A, Karwasz G P and Brusa R 1996 *Riv. Nuovo Cimento* **19** 1
[7] Visconti P, Slevin J and Rubin K 1970 *Phys. Rev.* A **3** 1310
[8] Jaduszliwer B and Chan Y C 1992 *Phys. Rev.* A **45** 197
[9] Brode R B 1929 *Phys. Rev.* **34** 673
[10] Bederson B and Kieffer L 1971 *Rev. Mod. Phys.* **43** 601
[11] Surdutovich E, Kauppila W E, Kwan C K, Miller E G, Parikh S P, Price K A and Stein T S 2004 *Nucl. Instrum. Methods.* B **221** 97
[12] Huang M-T, Zhang L, Hasegawa S, Southworth S H and Young L 2002 *Phys. Rev.* A **66** 012715
[13] Huang M-T, Wong W W, Inokuti M, Southworth S H and Young L 2003 *Phys. Rev. Lett.* **90** 163201
[14] Uhlmann L J, Dall R G, Truscott A G, Hoogerland M D, Baldwin K G H and Buckman S J 2005 *Phys. Rev. Lett.* **94** 173201
[15] Schappe R S, Keeler M L, Zimmerman T A, Larsen M, Feng P, Nesnidal R C, Boffard J B, Walker T G, Anderson L W and Lin C C 2002 *Adv. At. Mol. Opt. Phys.* **48** 357
[16] Raab E L, Prentiss M, Cable A, Chu S and Pritchard D E 1987 *Phys. Rev. Lett.* **59** 2631
[17] Wallace C D *et al* 1994 *J. Opt. Soc. Am.* B **11** 703
[18] Metcalfe H J and van der Straten P 1999 *Laser Cooling and Trapping* (New York: Springer)
[19] Bartschat K 1993 *J. Phys. B: At. Mol. Opt. Phys.* **26** 3595
Bartschat K and Fang Y 2000 *Phys. Rev.* A **62** 052719
Bartschat K 2002 Atomic and Molecular Data and Their Applications (*AIP Conference Proceedings* vol 636) ed D R Schultz, P R Krstic and F Owbny (New York: American Institute of Physics)
[20] Bartschat K 2005 Private Communication
[21] Chan S T and Gallagher A C 1978 *Phys. Rev.* A **17** 551